Electronic Supplementary Information

A novel strategy for realizing the high nitrogen doping in Fe_3C embedded nitrogen and phosphorus co-doped porous carbon nanowires: Efficient oxygen reduction reaction catalysis in acid electrolyte

Mian Li,[a,*] Yang Liu,[b] Lina Han,[b] Jie Xiao,[a] Xiaoyuan Zeng,[a] Chengxu Zhang,[a] Mingli Xu,[a] Peng Dong,[a] and Yingjie Zhang[*,a]

[a] *National and Local Joint Engineering Laboratory for Lithium-ion Batteries and Materials Preparation Technology, Key Laboratory of Advanced Battery Materials of Yunnan Province, Faculty of Metallurgical and Energy Engineering, Kunming University of Science and Technology, Kunming 650093, China.*

[b] *Faculty of Material Science and Engineering, Kunming University of Science and Technology, Kunming 650093, China.*

E-mail: mianzi2009@126.com, lim148@kmust.edu.cn (M. Li); zyjkmust@126.com (Y. Zhang)

1. Experimental Section.

Physical characterization of precursor networks and resultant control samples.

Wide-angle XRD patterns were obtained on an X-ray D/max-2200 vpc (Rigaku Corporation, Japan) instrument operated at 40 kV and 20 mA using Cu Kα radiation (*k* 0.15406 nm). SEM characterization was performed by using a Philips XL-30 ESEM equipped with an EDX analyzer. TEM analyses were performed on a high-resolution Hitachi JEM-2100 system. Surface analyses of resultant control catalysts were carried out by XPS on an ESCA LAB spectrometer (USA) using a monochromatic Al Kα source (*hv* 1486.6 eV). The binding energies were calibrated by using the containment carbon (C1s 284.6 eV). The N_2 adsorption-desorption isotherms were performed on an ASAP 2020 (Micromeritics, USA). Before the measurements, the samples were degassed in vacuum at 150 ℃ for 6 h. The Brunauer-Emmett-Teller (BET) method was utilized to calculate the BET specific surface area using adsorption data. The pore size distribution was derived from the adsorption branch by using the Barrett-Joyner-Halenda (BJH) model. Raman spectra were obtained using a confocal microprobe Raman system (HR800, JobinYvon).

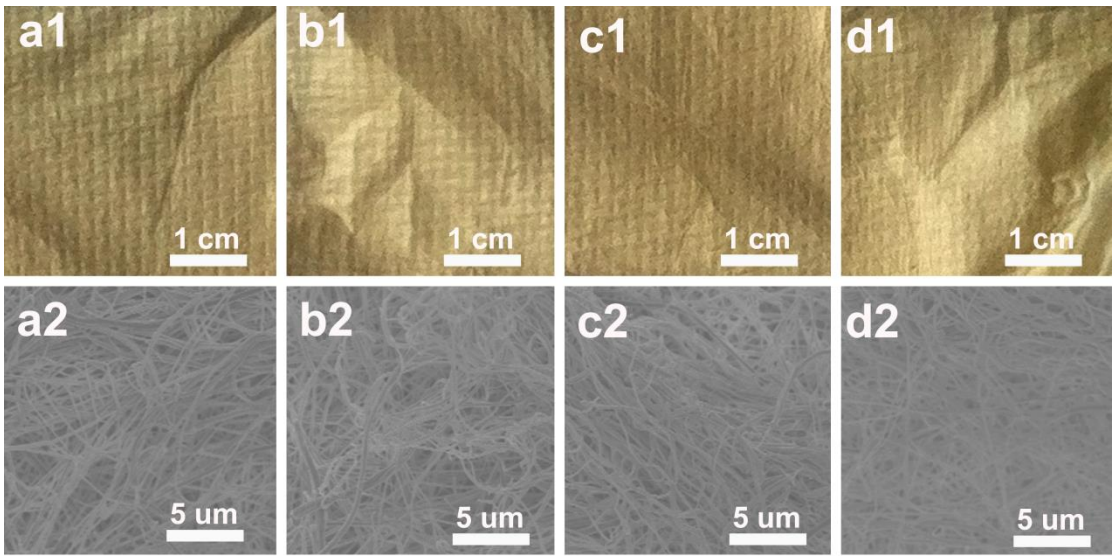

Fig. S1. The digital photographs **(a1-d1)** and SEM images **(a2-d2)** of as-wove 3D precursor networks for Fe_3C@PCFs **(a1, a2),** Fe_3C@N-PCFs **(b1, b2),** Fe_3C@P-PCFs **(c1, c2),** and Fe_3C@NP-PCFs **(d1, d2)** samples.

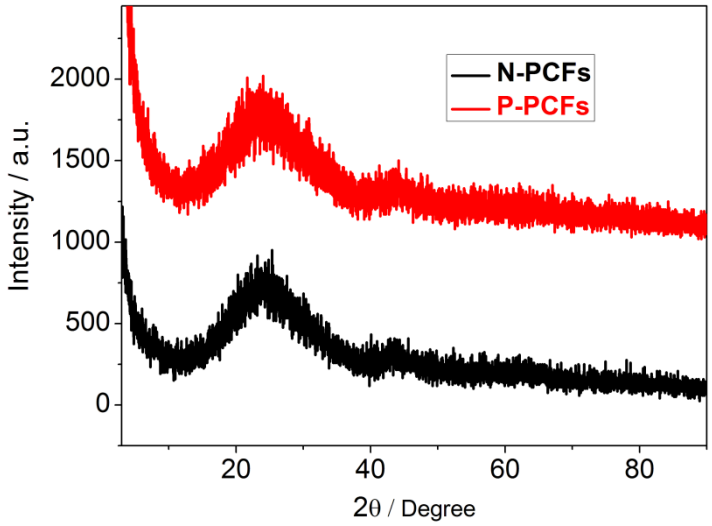

Fig. S2. The XRD patterns of resultant N-PCFs and P-PCFs samples.

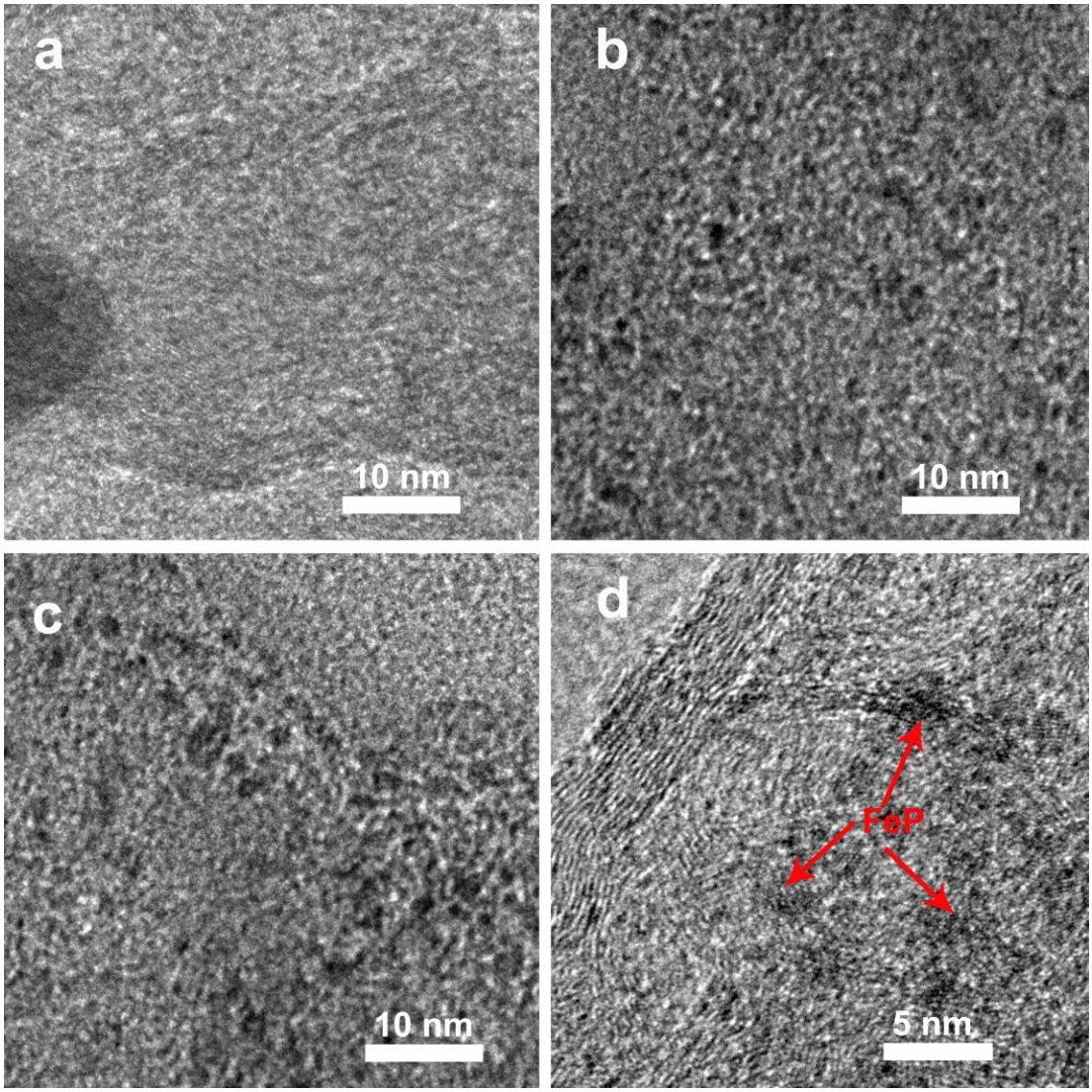

Fig. S3. HRTEM image of Fe_3C@N-PCFs (**a**), Fe_3C@P-PCFs (**b**) and Fe_3C@PN-PCFs (**c, d**) samples.

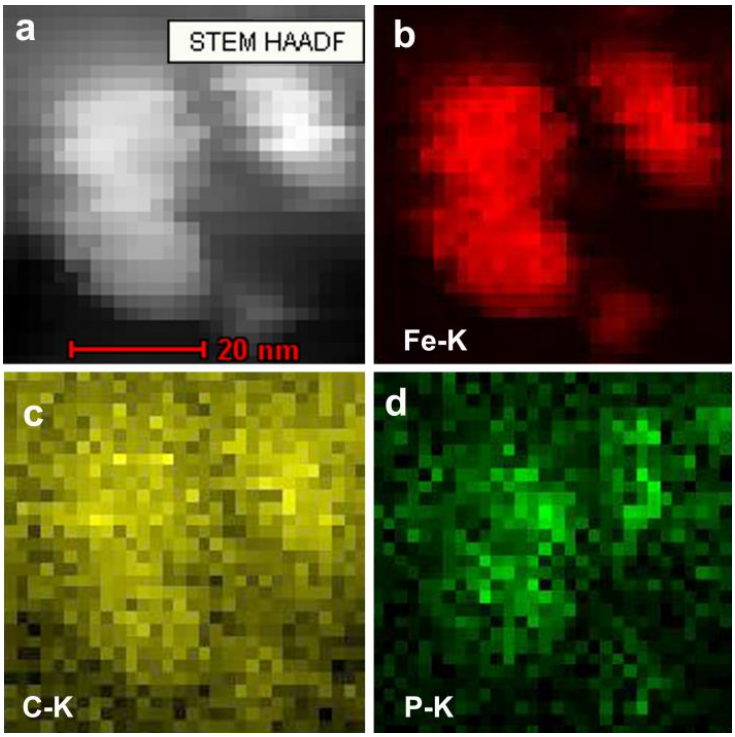

Fig. S4. Magnified HAADF-STEM image and corresponding EDS mapping of Fe, C and P elements for Fe_3C@P-PCFs sample**.**

The HAADF-STEM image and corresponding EDX elemental mapping images of Fe_3C@P-PCFs (**Fig. S4**) reveal that P and C elements were homogeneously dispersed along the catalyst's surfaces, indicating that P have successfully doped into the carbon matrices. For the large nanoparticles showed in STEM image (**Fig. S4a**), Fe-K (**Fig. S4b**) and C-K (**Fig. S4c**) curves all exhibit strong signals, demonstrating that the large nanoparticles are mainly existed in the form of Fe_3C. Furthermore, in the corresponding area, P-K curve (**Fig. S4d**) also exhibit P signals, which directly prove that the large Fe_3C nanoparticle is surrounded by P doped carbon layers. Especially, in addition to the P atoms dispersed along C, several bright spots with diameters less than 5 nm can also be observed in P-K curve (**Fig. S4d**); which demonstrates the existence of tiny FeP crystals.

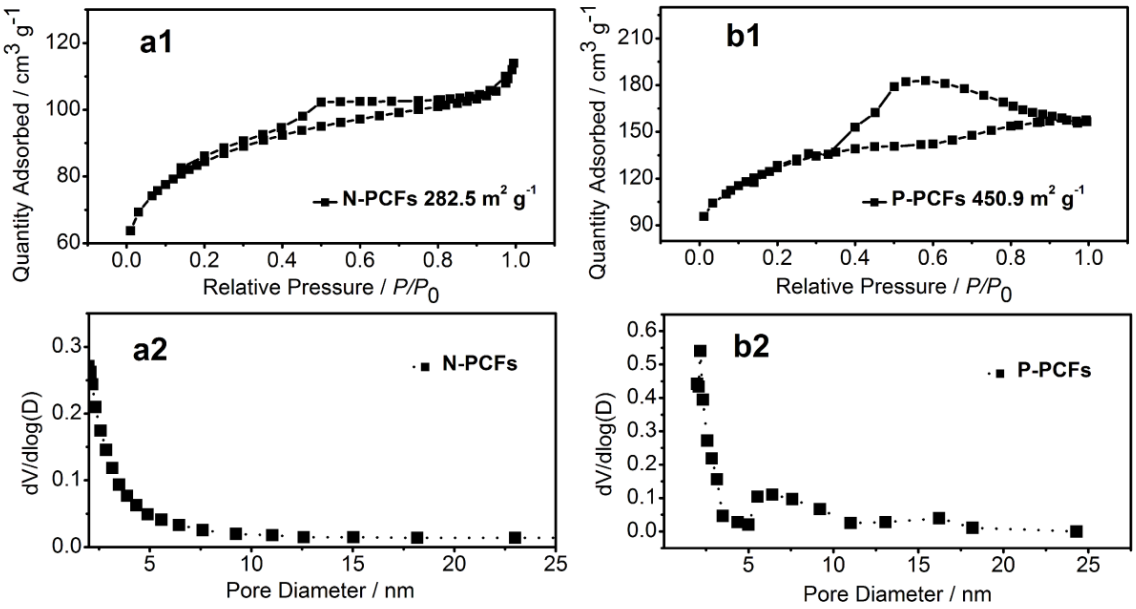

Fig. S5. The N_2 adsorption-desorption isotherms (**a1, b1**) and pore size distribution plots (**a2, b2**) of resultant N-PCFs **(a1, a2) and** P-PCFs **(b1, b2)** samples.

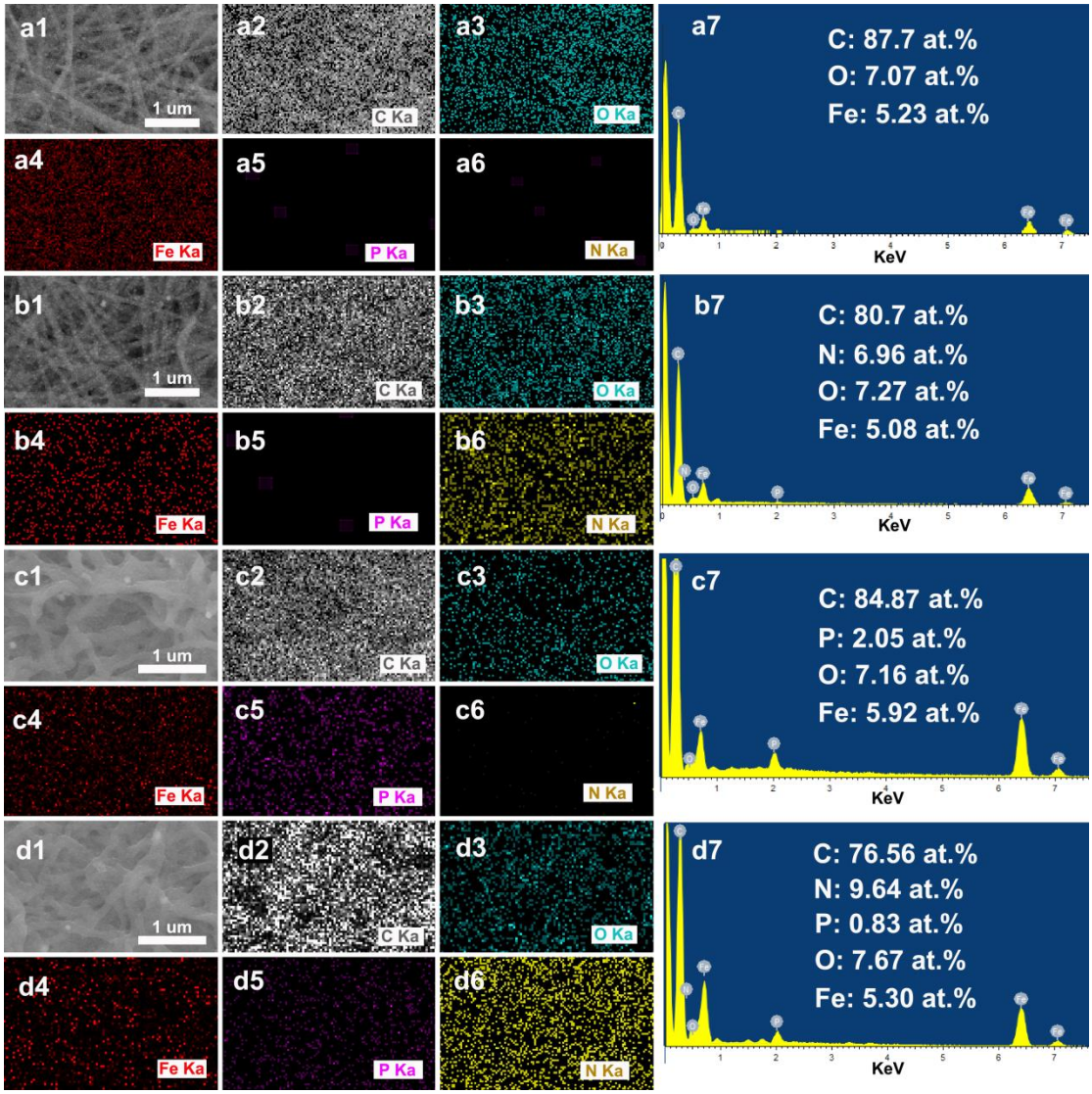

Fig. S6. SEM images (**a1, b1, c1, d1**), the corresponding C (**a2, b2, c2, d2**), O (**a3, b3, c3, d3**), Fe (**a4, b4, c4, d4**), P (**a5, b5, c5, d5**), N (**a6, b6, c6, d6**) element mapping images and EDX spectra (**a7, b7, c7, d7**) of resultant Fe_3C@PCFs (**a1-a7**), Fe_3C@N-PCFs (**b1-b7**), Fe_3C@P-PCFs (**c1-c7**) and Fe_3C@PN-PCFs (**d1-d7**) samples.

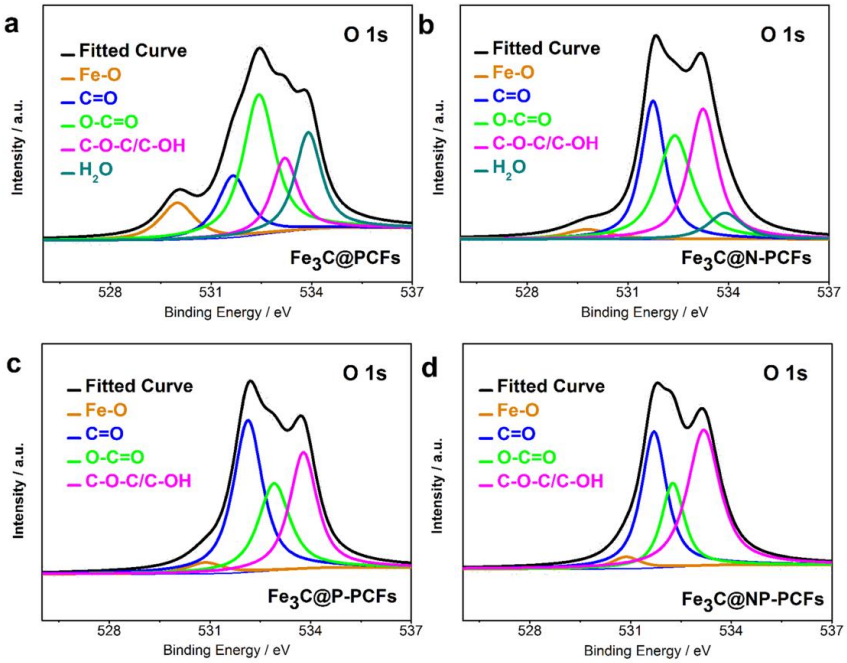

Fig. S7. The high-resolution O 1s spectra of resultant Fe_3C@PCFs **(a)**, Fe_3C@N-PCFs **(b)**, Fe_3C@P-PCFs **(c)** and Fe_3C@PN-PCFs **(d)** samples.

Table S1 The comparation of ORR catalytic parameters in 0.1 M KOH solution between our catalysts and other reported samples.

Samples	$\triangle E_{onset}$ [a] (mV)	$\triangle E_{1/2}$ [b] (mV)	References
Fe_3C@NP-PCFs	-15.6	+8.5	This work
Fe/P/C	-13	+6	Nano Energy 33 (2017) 221–228
Fe–N–C–800	~-50	~-45	J. Mater. Chem. A, 2018,6, 2527-2539
Fe–P-900	-20	-25	J. Am. Chem. Soc. 2015, 137, 3165−3168
Fe–N/C-800	-33	-9	J. Am. Chem. Soc. 136 (2014) 11027
Fe-N-CNFs	-30	-20	Angew. Chem. Int. Ed. 54 (2015) 8179 –8183
C-FeTA@g-C_3N_4	-	+40.0	J. Power Sources, 417 (2019) 117-124
NPMCS	-30	-19	J. Solid State Electrochem. 21 (2017) 103–110
NH_3-$Fe_{0.25}$-N/C-900	~-40	~-30	Nano Energy 36 (2017) 286–294
$Fe_3C@B_{1.0}$NPCFs	+14	+19	J. Colloid Interf. Sci. 533 (2019) 709-722
Co-C@NWCs	～-10	+20	Small 12 (2016) 2839–2845
Co@Co_3O_4/NC-1	～-180	-10	Angew. Chem. Int. Ed. 55 (2016) 4087 –4091
Co, N-CNF	-7	+20	Adv. Mater. 28 (2016) 1668–1674
HLCT-1/2	+10	+57	Adv. Funct. Mater. 2019, 1900015
Fe-Cu-N/C	+25	+50	Nano Energy 37 (2017) 187–194
Co_{1-x}S/N-S-G	+16	+30	J. Mater. Chem. A 5 (2017) 12354-12360
PAC-5S	-90	-60	J. Mater. Chem. A, 5 (2017) 1742-1748
AC-F-U-P	-70	-100	Appl. Catal. B-Environ. 204 (2017) 394–402

As the commercial Pt/C is the state-of-the-art ORR catalyst and have been chosen as the reference in all previous papers. For fairly comparing the catalytic parameters of different catalysts reported in different papers and simultaneously avoiding the errors caused by different instruments or different researchers' operations:

[a] **$\triangle E_{onset}$ ($\triangle E_{onset}$=E_{onset} for resultant catalyst - E_{onset} for Pt/C);**

[b] **$\triangle E_{1/2}$ ($\triangle E_{1/2}$ =$E_{1/2}$ for resultant catalyst - $E_{1/2}$ for Pt/C)**.

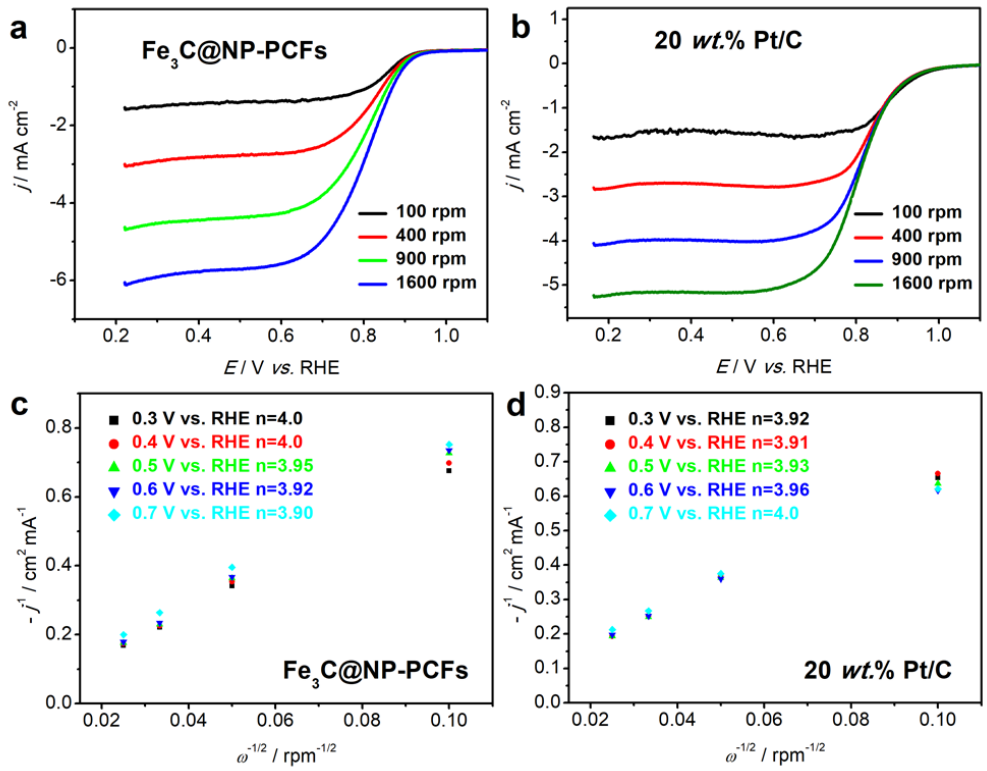

Fig. S8. LSV polarization curves of Fe_3C@NP-PCFs (**a**) and 20 *wt.*% Pt/C (**b**) catalysts measured in O_2-saturated 0.1 M KOH at various rotation speeds from 100 rpm to 1600 rpm at scan rate of 5 mV s^{-1}. The corresponding *K-L* plots of Fe_3C@NP-PCFs (**c**) and 20 *wt.*% Pt/C (**d**) catalysts. LSVs were obtained by scanning the potential from 1.10 to 0.20 V *vs.* RHE at various rotation speeds.

The corresponding Koutecky–Levich (*K–L*) plots (j^{-1} *vs.* $\omega^{-1/2}$) derived from the RDE voltammograms (**Fig. S8a, 8b)** according to the equations expressed as **eqn. S1** and **eqn. S2** are presented in **Fig. S8c, 8d**. The *K–L* plots are usually used to assess the apparent electron transfer numbers (*n*) during the ORR:

$$\frac{1}{j} = \frac{1}{j_k} + \frac{1}{j_L} \qquad \textbf{(S1)}$$

$$j_L = 0.62nFAD^{2/3}\nu^{-1/6}\omega^{1/2}C_{O_2} \qquad \textbf{(S2)}$$

Herein, j, j_k and j_L are the measured, kinetic, and diffusion limiting current densities (mA cm^{-2}), respectively. The n value is the number of electrons transferred during the ORR and is extracted from the slope, F is the Faraday's constant (96485 C mol^{-1}). D is the diffusion coefficient for oxygen (1.9×10^{-5} cm^2 s^{-1}), ν is the kinetic

viscosity (1.13×10^{-2} cm^2 s^{-1}), ω is the rotation rate of electrode (rpm), C_{O_2} is the bulk concentration of oxygen dissolved in the electrolyte (1.2×10^{-3} mol m^{-3}).

The *K–L* plots at various potentials exhibit good linearity and parallelism for the Fe_3C@NP-PCFs and 20 *wt.*% Pt/C catalysts in 0.1 M KOH (**Fig. S8a, 8b**), indicating the first-order reaction kinetics for ORR with respect to the concentration of dissolved oxygen in 0.1 M KOH. The *n* values for the two catalysts at different potentials were calculated and recorded in **Fig. S8c, 8d**. It is clear that the *n* values calculated between 0.3-0.7 V *vs.* RHE are between 3.90-4.00 for Fe_3C@NP-PCFs and 20 *wt.*% Pt/C catalysts in 0.1 M KOH, respectively, which demonstrates a dominant 4 e^- transfer pathway for the Fe_3C@NP-PCFs catalyst in 0.1 M KOH, similar to ORR catalyzed by the state-of-the-art Pt/C catalyst.

Table S2 The comparation of catalytic parameters in 0.5 M H_2SO_4 solution between our catalysts and other reported samples.

	$\triangle E_{onset}$ [a] (mV)	$\triangle E_{1/2}$ [b] (mV)	References
Fe_3C@NP-PCFs	-10.1	-27.7	This work
Fe_3C@$B_{1.0}$NPCFs	-40	-50	Journal of colloid and interface science, 2019, 533, 709-722
TM-N-C	-70	-90	Small, 2014,10, 4072-4079
Fe/P/C networks	-56	-70	Nano Energy, 2017, 33, 221–228
Fe–N–C/VA-CNT	～-50	～-50	Adv. Funct. Mater. 2016, 26, 738
Fe_3C@NCNF-900	-153	-149	ACS Appl. Mater. Interfaces 2016, 8, 4118−4125
Fe−P-900	～-180	～-300	J. Am. Chem. Soc. 2015, 137, 3165
LDH@ZIF-67-800	～-50	-	Adv. Mater. 2016, 28, 2337–2344
pPMF-800	-84	-72	Nanoscale, 2016, 8, 959–964
Fe-N-CNFs	～-100	～-150	Angew. Chem. Int. Ed. 2015, 54, 8179 –8183
Fe_3C/NCNTs/ OBP-900	～-100	～-100	J. Mater. Chem. A, 2015, 3, 21451–21459
Fe_3C/NG-800	～-100	～-100	Adv. Mater. 2015, 27, 2521–2527
Fe−N/C-800	-38	-59	J. Am. Chem. Soc. 2014, 136, 11027−11033
PMF-800	-44	～-180	J. Am. Chem. Soc. 2015, 137, 1436−1439

As the commercial Pt/C is the state-of-the-art ORR catalyst and have been chosen as the reference in all previous papers. For fairly comparing the catalytic parameters of different catalysts reported in different papers and simultaneously avoiding the errors caused by different instruments or different researchers' operations:

[a] **$\triangle E_{onset}$ ($\triangle E_{onset}$=E_{onset} for resultant catalyst - E_{onset} for Pt/C);**

[b] **$\triangle E_{1/2}$ ($\triangle E_{1/2}$ =$E_{1/2}$ for resultant catalyst - $E_{1/2}$ for Pt/C)**.

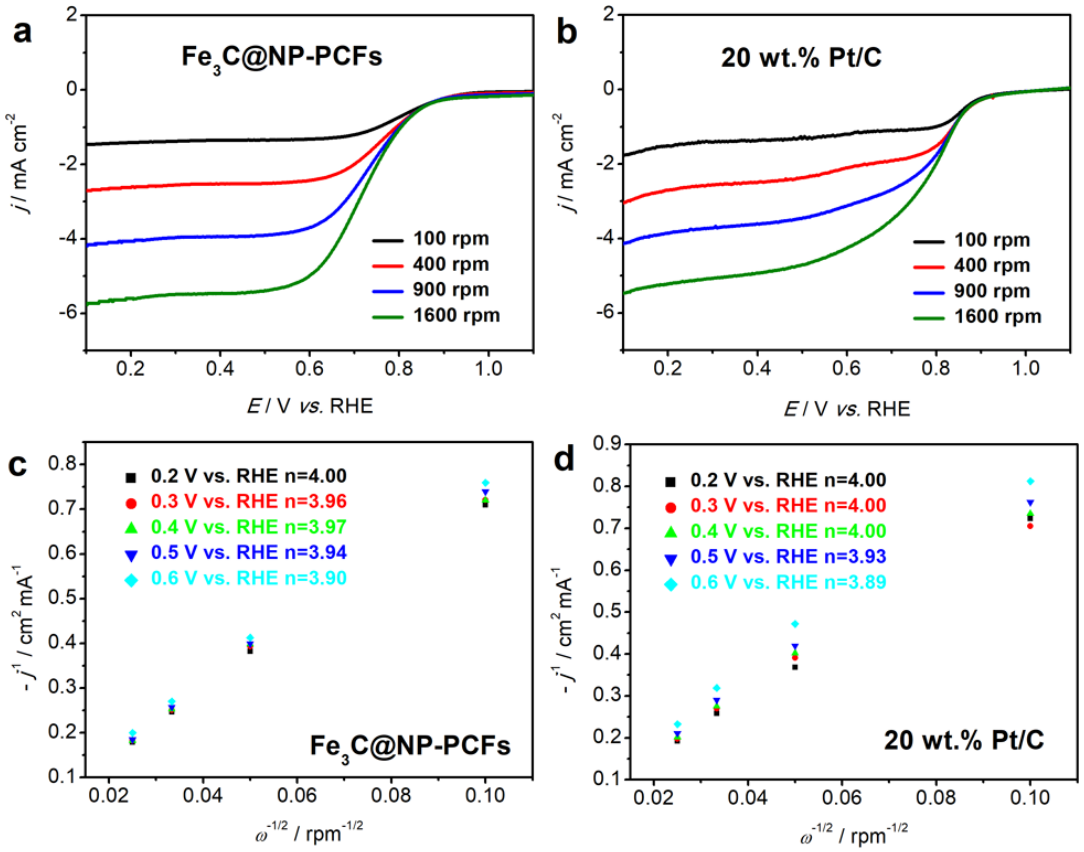

Fig. S9. LSV polarization curves of Fe_3C@NP-PCFs (**a**) and 20 *wt.*% Pt/C (**b**) catalysts measured in O_2-saturated 0.5 M H_2SO_4 at various rotation speeds from 100 rpm to 1600 rpm at scan rate of 5 mV s^{-1}. The corresponding *K-L* plots of Fe_3C@NP-PCFs (**c**) and 20 *wt.*% Pt/C (**d**) catalysts. LSVs were obtained by scanning the potential from 1.10 to 0.10 V *vs.* RHE at various rotation speeds.

The corresponding *K–L* plots (j^{-1} *vs.* $\omega^{-1/2}$) derived from the RDE voltammograms in 0.5 M H_2SO_4 (**Fig. S9a, 9b)** according to the equation expressed as **eqn. S1** and **eqn. S2** are presented in **Fig. S9c, 9d**. The *K–L* plots at various potentials also exhibit good linearity and parallelism for the Fe_3C@NP-PCFs and 20 *wt.*% Pt/C catalysts in 0.5 M H_2SO_4, indicating the first-order reaction kinetics for ORR with respect to the concentration of dissolved oxygen in 0.5 M H_2SO_4. The *n* values of two catalysts at different potentials were calculated and recorded in **Fig. S9c, 9d**. It is clear that the *n* values calculated between 0.2-0.6 V *vs.* RHE are between 3.90-4.00 for Fe_3C@NP-PCFs and 20 *wt.*% Pt/C catalysts in 0.5 M H_2SO_4, respectively; which demonstrates a dominant 4 e^- transfer pathway for the Fe_3C@NP-PCFs catalyst in 0.5 M H_2SO_4, similar to ORR catalyzed by the state-of-the-art Pt/C catalyst.

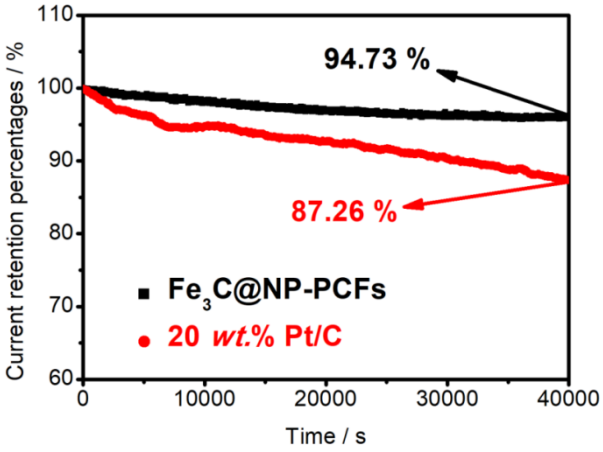

Fig. S10. The chronoamperometric responses of Fe_3C@NP-PCFs and 20 wt.% Pt/C catalysts in O_2-saturated 0.5 M H_2SO_4 solution recorded at 0.65 V *vs.* RHE with a rotation rate of 900 rpm.

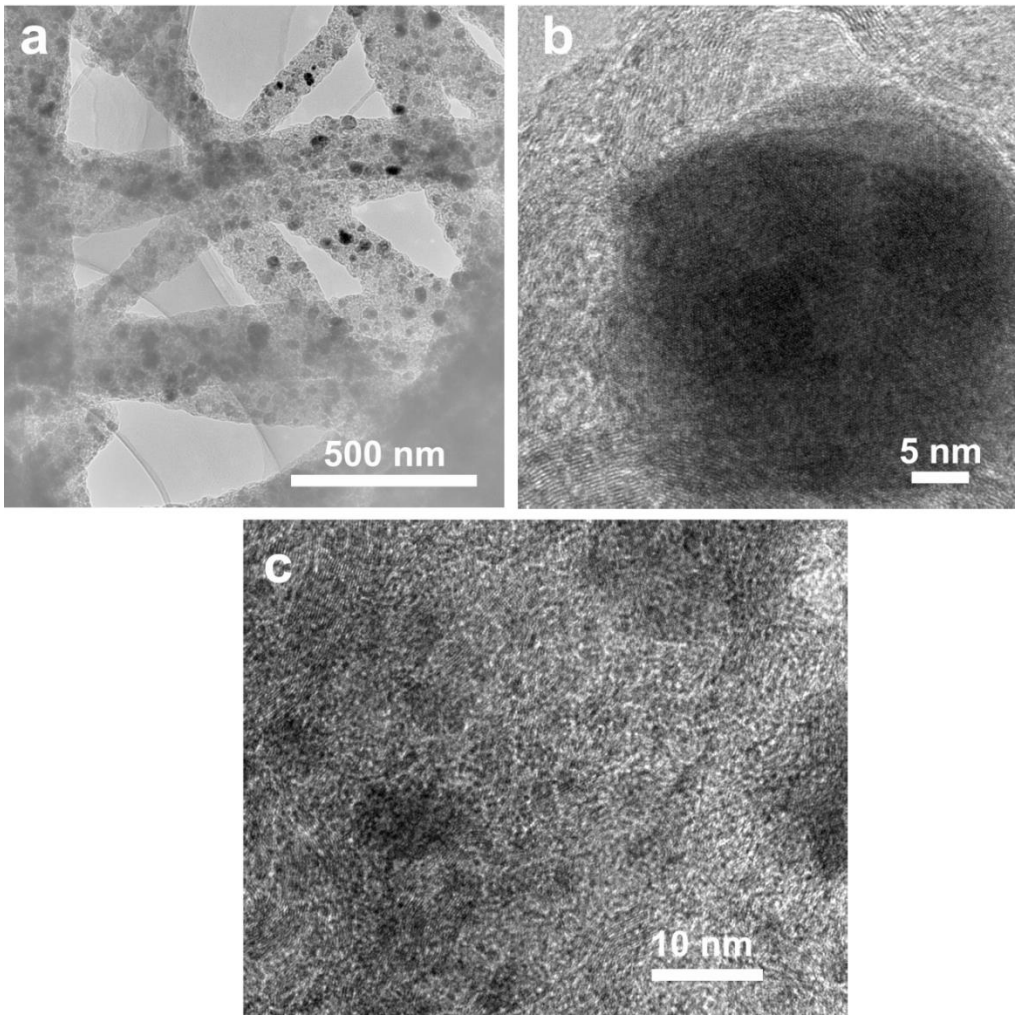

Fig. S11. LSV polarization curves of Fe_3C@NP-PCFs (**a**) and 20 *wt.*% Pt/C (**b**) catalysts measured in O_2-saturated 0.5 M H_2SO_4 at various rotation speeds from 100 rpm to 1600 rpm at scan rate of 5 mV s^{-1}. The corresponding *K-L* plots of Fe_3C@NP-PCFs (**c**) and 20 *wt.*% Pt/C (**d**) catalysts. LSVs were obtained by scanning the potential from 1.10 to 0.10 V *vs.* RHE at various rotation speeds.

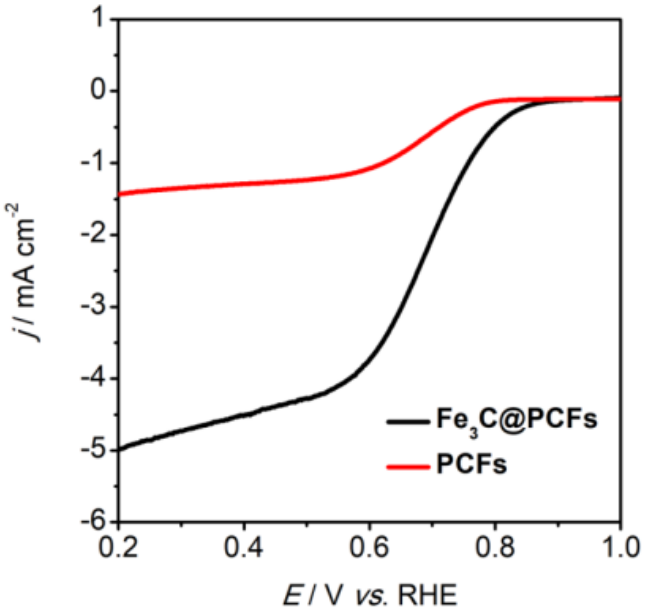

Fig. S12. The ORR LSV polarization curves of PCFs and Fe_3C@PCFs control samples in 0.1 M KOH.